MC calculations for the nEDM experiment systematics

K. Bodek[a], Z. Chowdhuri[b], M. Daum[b,c], M. Fertl[b], B. Franke[b,d], E. Gutsmiedl[e], R. Henneck[b], M. Horras[b,d], M. Kasprzak[f], K. Kirch[b,g], S. Kistryn[a], A. Kozela[a], J. Krempel[b], B. Lauss[b], A. Mtchedlishvili[b], F. Piegsa[g], G. Pignol[h], D. Rebreyend[h], S. Roccia[i], P. Schmidt-Wellenburg[b], J. Zejma[a], J. Zenner[b,j], G. Zsigmond[b]*

[a]*Marian Smoluchowski Institute of Physics, Jagiellonian University, 30–059 Cracow, Poland*
[b]*Paul Scherrer Institut, CH-5232 Villigen PSI, Switzerland*
[c]*Physics Department, University of Virginia - Charlottesville, VA, USA*
[d]*Excellence Cluster "Universe", Technische Universität München - D-85748 Garching, Germany*
[e]*Physics Department E18, Technische Universität München, D-85748 Garching, Germany*
[f]*FRAP, University of Fribourg, CH-1700 Fribourg, Switzerland*
[g]*ETH Zürich, CH-8093 Zürich, Switzerland*
[h]*LPSC, Université Joseph Fourier Grenoble 1, CNRS/IN2P3, Institut National Polytechnique de Grenoble 53 F-38026 Grenoble Cedex, France*
[i]*Instituut voor Kern-en Stralingsfysica, Katholieke Universiteit Leuven - B-3001 Leuven, Belgium*
[j]*Johannes-Gutenberg-Universität - D-55128 Mainz, Germany*

Abstract

The nEDM experiment hosted at the Paul Scherrer Institute is the flagship project at the new ultracold neutron facility. Estimations of systematic effects for the determination of the neutron electric dipole moment play an important role in this project. Experimental studies are supported by Monte Carlo simulations using the MCUCN code. Here we briefly present first results on the experimental benchmark of the model, and on the evaluation of the storage time dependence of the centre of mass of UCN in the nEDM precession chamber. Such time dependence calculations will serve as consistency tests for future measurements involving field gradient corrections of the Ramsey resonance frequency. An analytic benchmark of the spin-handling routines will also be shown.

Keywords: ultracold neutrons, neutron electric dipole moment, MC simulations

1. Introduction

The new ultracold neutron (UCN) source at the Paul Scherrer Institute (PSI) started its operation December 2010. The nEDM (neutron electric dipole moment) experiment is the flagship project at this new facility. Details are reported in these proceedings [1].

Estimations of the size of systematic effects in the determination of the neutron EDM play an important role in this experiment. Specific experimental studies are supported by Monte Carlo simulations serving as consistency

* *Corresponding author*: Tel.: +41-56-310-3569. *E-mail address*: geza.zsigmond@psi.ch

tests and helping to estimate the size of the corrections. The aim for the Monte Carlo is to develop a full realistic model of the PSI UCN source, UCN guides, and nEDM apparatus, using parameterizations of measured magnetic field maps, including spin transport and Ramsey cycles.

The presented simulations of the nEDM apparatus [2] as operated at PF2/ILL are an important step in benchmarking our MC code for future computations of the experiment installed at the PSI source. Furthermore, results of an application of the simulation code are presented: the evolution in time of the time averaged center of mass (CM) of UCNs in the apparatus at PF2/ILL. First test results of the spin-handling routines are also included.

2. Features of the MCUCN code

The MCUCN code used in this work was developed within the UCN physics group at PSI. It includes all pertinent geometry details of the UCN source storage volume, guides and precession chamber system. It uses second-order shaped surfaces. Time dependent shutters are defined and disc choppers for time-of-flight calculations. UCN are represented by time, position, velocity and spin vector coordinates. Gravity, which plays an important role in UCN dynamics, is implemented in the code. In contrast to GEANT4, the parabolic trajectories are analytically calculated between successive reflection or transmission points, thus the code is very fast.

Spin precession is calculated from the Bloch equations (if this option is switched on) along the analytical trajectory with fourth order Runge-Kutta (RK4) and adaptive stepsize methods. One step means a step in time along the trajectory. The required precision of the algorithm can be set as an input parameter. It is defined as the maximal allowed error per step for each spin vector component. It is typically between 10^{-6} - 10^{-8}. The error is calculated by comparing the new spin after one full step and after two half steps. If the error of one of the x, y, or z components is larger than the stepsize will be reduced and a new iteration is done.

The RK4 approach is rather slow therefore implementation of RK8-9 is planned.

Between reflection or transmission points, the spin has no influence on the trajectory. Thus the code works with the limitation that on a free path the magnetic potential must be negligible compared to the kinetic energy. However, fair approximations are valid for polarizers and analyzers: (i) a magnetic polarizing foil is simulated by making the Fermi potential spin dependent; (ii) the superconducting magnet polarizer on the PSI nEDM beamline is approximated by a rectangular potential energy barrier.

The incorporated physical properties of the interacting surfaces are

- Fermi optical potential V_F;
- A loss constant $\eta = W_{loss}/V_F$, (from absorption, and up-scattering) which enters the energy and direction dependent reflectivity Eq. 2.71 in Ref. [3]
- Diffusivity models:
  - Weighting the specular reflection and the Lambert-model as in Ref. [3] p.100., the projection of the reflected direction to the surface normal ($\cos\theta$) is linearly distributed; the fraction of diffuse reflections will be noted by $p_{diffuse}$. This approach is applicable for macroscopic surface irregularities and cavities;
  - Micro-roughness model describing interference of reflected waves according to Ref. [4]. This is applicable only for highly polished surfaces.
- Attenuation parameter for transmission (product of macroscopic attenuation constant [cm^{-1}] and thickness) as a function of the velocity inside the medium (v_{foil}). Partial reflection at the exiting surface of the foil (thickness $\gg$ UCN wavelength) is also considered using probability $T = 4v_{vac}v_{foil}/(v_{vac}+v_{foil})^2$ for transmission (see p. 138 in Ref. [5]);
- Spin flip probability per collision.

3. MCUCN calculations for the nEDM apparatus at PF2/ILL

The following results consider the nEDM apparatus operated at PF2/ILL. The main components used for the simulation model in the following two subsections are depicted in Fig. 1.

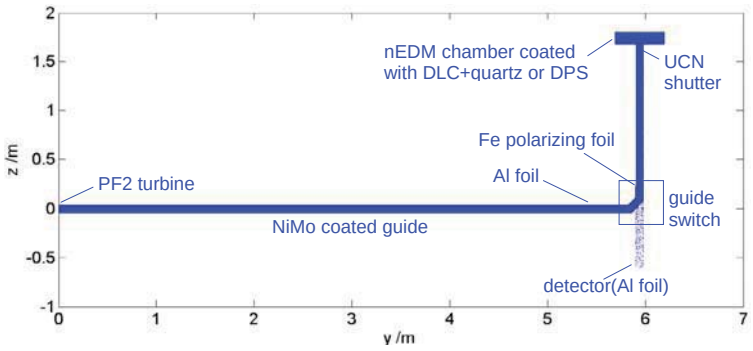

Fig.1: Simplified scheme of the simulated apparatus at ILL. The blue shadings are computed wall reflections (dots) during a whole cycle.

The flux distribution of the PF2/ILL turbine source was approximated by a linear kinetic energy distribution up to 400 neV, a homogeneous 2-dimensional spatial distribution, cosine angular distribution, and an equal distribution of up and down spin states corresponding to an unpolarized beam. The upper part of the energy spectrum is shaped by the optical potential of the horizontal (V_F = 380 neV) and vertical (V_F = 250 neV) guides.

The optical potential of the polarizing Fe foil was defined to be spin dependent (90 neV and 330 neV). In all calculations here depolarization on the surfaces was switched off. The optical potential of the isolator ring was 95 neV for quartz if not otherwise indicated.

The filling, storage, and emptying phases were simulated by switching instantly the appropriate on and off states of the UCN shutter at the entrance of the chamber. An important issue – the effect of the movement of the real shutter – has not been simulated up to now; however, this can be done in the current version by using a discrete set of shutter positions switched on and off in succession (flip book principle). In a next version of MCUCN the disc chopper feature will be extended to also include linear i.e. shutter motion.

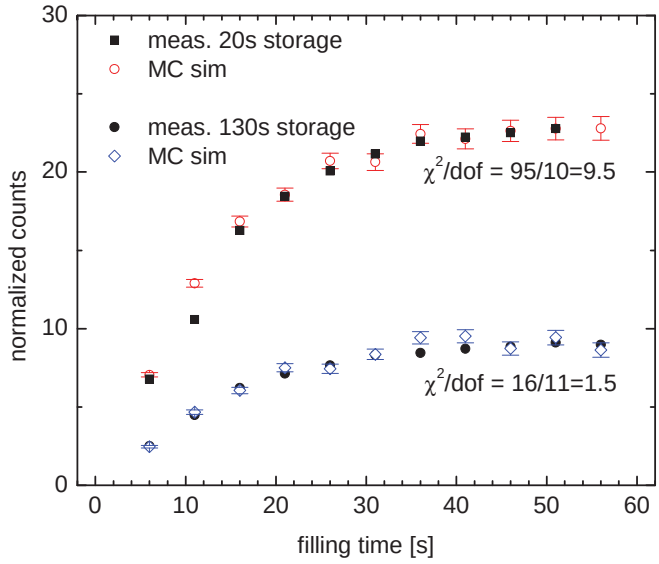

Fig. 2: UCN counts versus filling time: comparing measurement and simulation with one global normalization for 20 s and 130 s storage time. At the data point 20 s storage time and 11 s filling time the discrepancy is 9.2 σ, by excluding this data point, the average discrepancy (see text) becomes 1.1 σ.

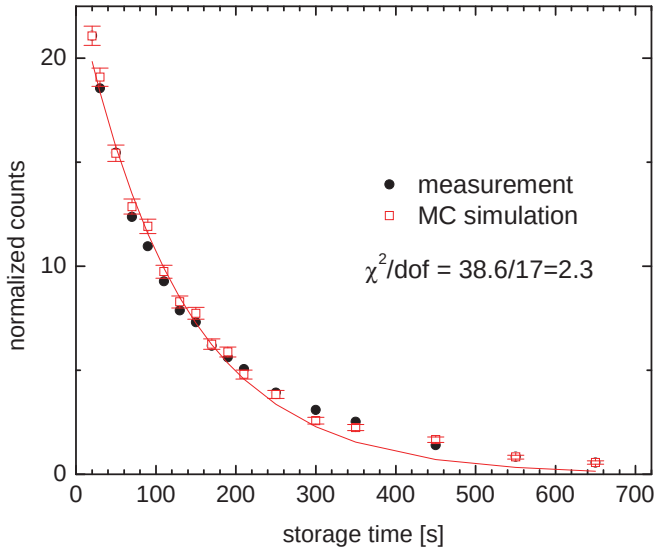

Fig. 3: UCN counts as function of storage time: comparing measurement and simulation. Deviation of the data points from a single exponential line is visible, as expected for a wide range of kinetic energy.

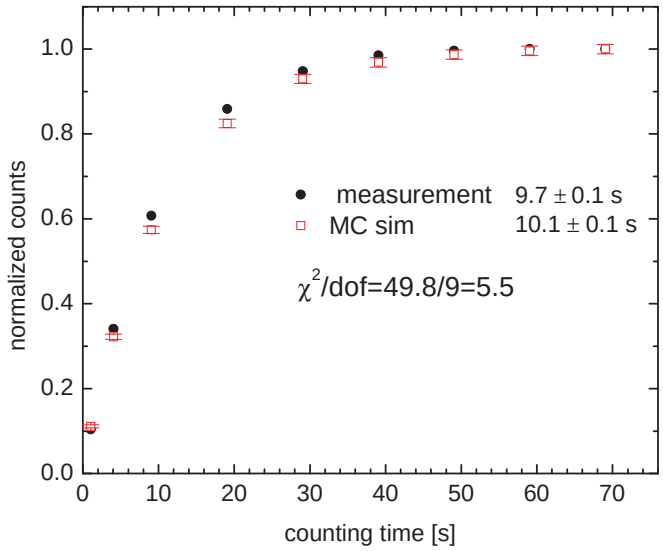

Fig. 4: UCN counts as function of emptying time: comparing measurement and simulation. The two time constants obtained from single exponential fits are very close.

The diffuse reflections from walls were calculated using the Lambert law. This choice was based on our first comparison series of UCN storage and emptying simulations where the micro-roughness model gave emptying time profiles that were indistinguishable from those using the Lambert model with a diffuse fraction much less than 1 %. This weak effect was in contradiction with the fact that surface profiles and cavities cause a diffuse fraction in the system larger than 1% as estimated from the fraction of the total surface.

3.1. Benchmark of the model against experiments

The simulations presented here for the nEDM apparatus at PF2/ILL represent a step in benchmarking our MC code. Routines developed here to compare MC and experimental results will allow for more profound predictions for the nEDM apparatus at PSI. Counting rates at the detector were simulated in the way they were measured for different sets of filling, storing and emptying times of the UCN precession chamber (see Ref. [6], [7]).

Wall-loss (η) and diffusivity (p_{diffuse}) parameters were tuned by several manual iterations. MC results shown in Figs. 2–4 were calculated with fixed surface and transmission parameters (see Sec. 2).

As an initial iteration value, the MC counts normalization was done and fixed at the highest endpoints of the measured curves and kept the same for one type of data (filling, storage, or emptying). With this normalization parameter we adjust the UCN density from the MC to the measured density.

As a figure of merit for the MC data we calculate the χ^2 and divide by the number of data points (n). This was done in the following way: For each data point we can define the deviation of MC value from the measurement in multiples of the standard deviation σ of the MC. The square root of χ^2/n gives thus a statistical average of these values. The measurements had high statistics thus these errors were negligible in χ^2 beside the σ of the MC.

By manually minimizing χ^2 we obtain in the chamber $\eta = (4.0\pm0.2)\times10^{-4}$ and $p_{\mathrm{diffuse}} = 0.10\pm0.05$. The next manual iteration procedure, namely, setting the coating parameters fixed and tuning the density normalization parameter, was not yet done.

Further fine-tuning is in progress with the development of an automatic procedure to be able to scan a larger parameter space and to adjust the density normalization parameter with better resolution. The routines written for matching the MC data to experimental data will be adapted in the simulation of measurements at the PSI source. An important issue, the movement of the UCN shutter at the entrance of the chamber will be included and allow a better description of the apparatus behaviour.

3.2. UCN center of mass calculation

Precise computations of the difference between the center of mass of UCN and ^{199}Hg-atoms (as cohabiting magnetometer) serve as an important input for consistency tests for magnetometer measurements. It can be directly related to the vertical gradient of the magnetic field and thus used for the determination of false EDM contributions. The CM of particles is defined in this work as the time average of the vertical position during storage time averaged over all UCNs.

The centre of mass offset is caused by gravity and the large speed difference between UCN (~5 m/s) and Hg atoms (~150 m/s) of the co-magnetometer [2]. This offset determines the ratio of precession frequencies measured for UCN and mercury atoms as function of a vertical magnetic field gradient. Namely, as indicated in [8], a CM offset of the Hg and UCN pulls the frequency ratios away from the ratio of gyromagnetic factors:

(1) $$\frac{\omega_{Ln}}{\omega_{\mathrm{LHg}}} = \left|\frac{\gamma_n}{\gamma_{\mathrm{Hg}}}\right|\left(1 - \frac{\Delta z}{B_{0z}}\frac{\partial B_z}{\partial z}\right)$$

The CM offset Δz is involved in specific false EDM contributions caused by magnetic field gradients [2].

Two Fermi potentials for the insulator ring of the nEDM chamber were considered in the simulations: V_F =95 neV for quartz and V_F =162 neV for deuterated polystyrene (dPS) [9]. The offsets of the center of mass of UCNs as a function of storage time are given in Fig. 5.

In Fig. 5 the CM offset is increasing with storage time. This can be explained in the following way. The loss per bounce is defined in MCUCN by the theoretical prediction Eq. 2.71 from Ref. [3]. This results in a higher loss for higher energy UCN. Since the collision rate is also larger for faster particles, the average kinetic energy of stored UCN will decrease with time due to wall losses. To illustrate this, the calculated dependence of the time averaged kinetic energy on the storage time is shown in Fig. 6.

For quartz, we computed a 2.8 mm shift at 60 s. This shift value was, however, obtained experimentally in Ref. [2] for a larger storage time 130 s. Also recent measurements show a much smaller slope for the CM storage time dependence than plotted in Fig. 5. We assume that these discrepancies originate from a more complicated change of the energy spectrum during storage than as described in the previous paragraph. This situation will be further studied.

As a consistency test, in Fig. 7 it is shown that ergodicity is fulfilled, which means that the ensemble average of the vertical positions $\langle z \rangle_{ens}$ in the chamber is equal to its time average $\langle z \rangle_T$. Since we deal with a large number of UCN, the time average CM is calculated in our case as the ensemble average of the individual time averages $\langle\langle z \rangle_T \rangle_{ens}$.

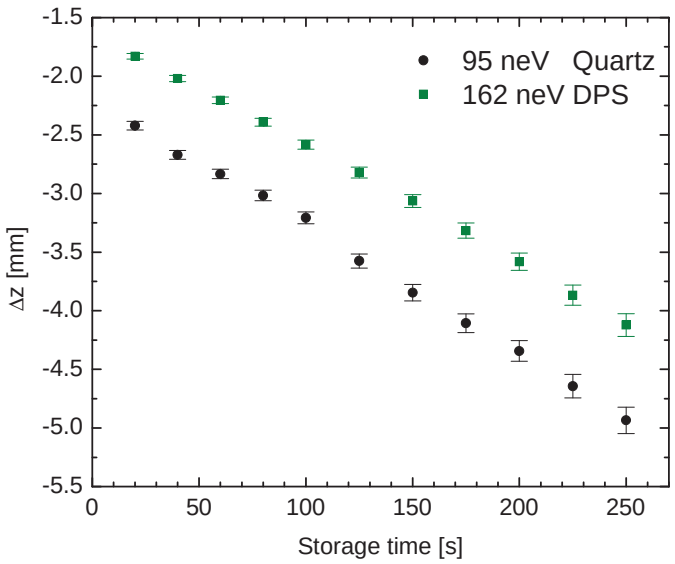

Fig.5: Calculated dependence of the offset of the CM Δz (relative to the chamber centre) on the storage time for quartz and dPS.

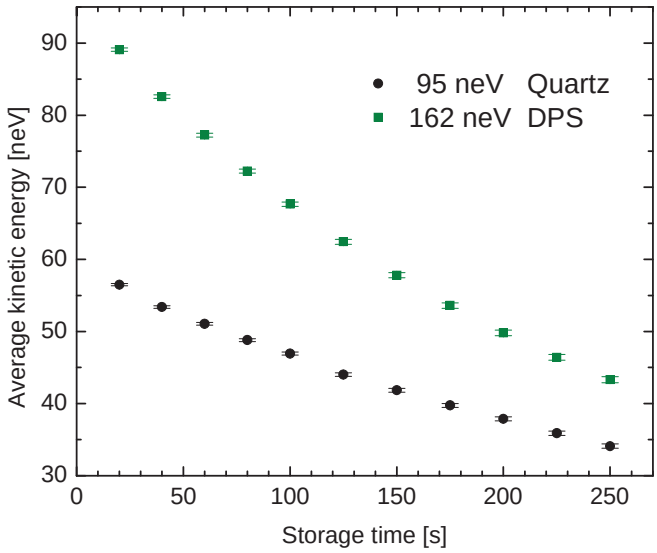

Fig. 6: Calculated dependence of the time averaged kinetic energy, also averaged over all UCN, on storage time. Faster UCN will be lost due to more frequent collisions.

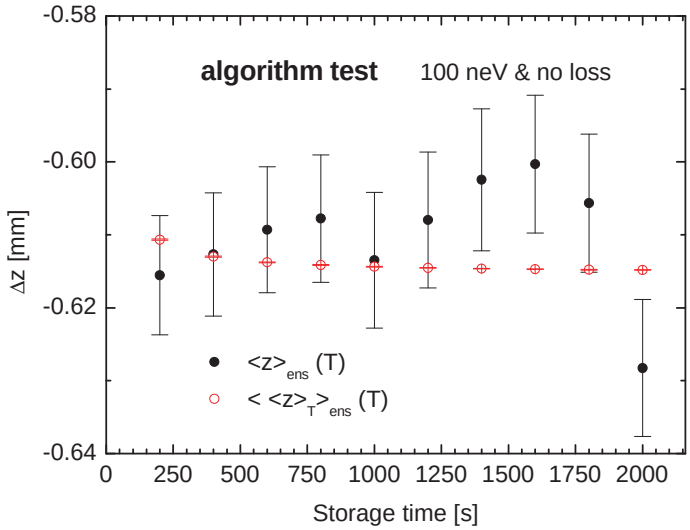

Fig. 7: Algorithm test of ergodicity at large times (see text). Losses were switched off in order reduce CPU time and to reach high statistics.

4. Spin handling and preliminary results

A typical Ramsey cycle as in the real nEDM experiment was recently implemented in the MCUCN model as illustrated in Fig. 8. The RK4 method with adaptive stepsize was used to solve the Bloch equations.

Any kind of time, position and velocity dependent (via $\mathbf{v}\times\mathbf{E}$) magnetic field can be used in analytical form in this code. Parametrization is obtained by fitting the field maps measured at PSI with a routine written for this purpose using spherical harmonics.

In the short example presented here, a typical constant vertical gradient magnetic field, $\partial_z B_z$ was considered. We consider the case that the magnetic field has rotational symmetry around the z axis. Thus the radial field components are obtained from the Maxwell equation $\nabla\cdot\mathbf{B} = 0 \Rightarrow \partial_{x,y}B_{x,y} = -1/2\times\partial_z B_z$. For the present test purpose, in order to obtain reasonable statistics in several nights on a computing grid [10], only the volume of the precession chamber was considered and a linear initial energy spectrum. The allowed uncertainty for the spin component calculation per one RK4 step was set to 10^{-6}. Depolarization at surface collisions was switched off in order to separate transversal depolarization.

In Fig. 9 we zoom to the resonance frequency in the center of the Ramsey curve, and show the cases when gravity is switched on and off at a gradient 400 pT/cm. By fitting a squared cosine function [7] around the resonance point, the UCN frequency shift can be obtained. This amounts to $(3.8\pm1.5)\times10^{-5}$.

As deducible from Eq.(1), the relative shift when switching on gravity is due to the center of mass offset and the field gradient as given by the formula $\Delta\omega_{Ln}/\omega_{Ln} = -\Delta z\partial_z B_z/B_z$. A simulation of Δz with the conditions described above yields a relative frequency shift $(5.0\pm2.8)\times10^{-5}$.

The two above results are very close and serve as an analytic benchmark for the MC. The precision will be improved by setting the allowed uncertainty for spin component calculation per RK4 step to 10^{-7}.

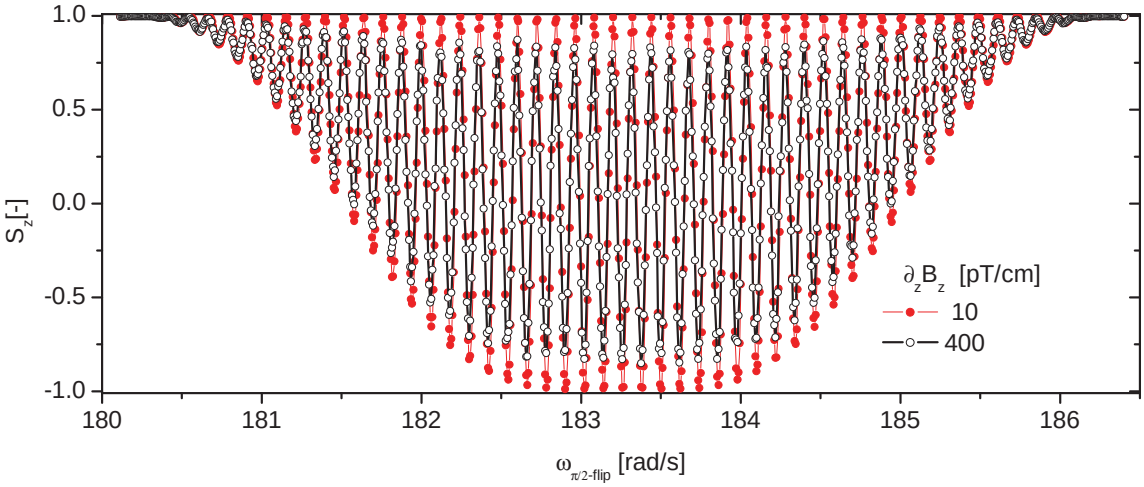

Fig.8: Typical nEDM Ramsey cycle for 50 s precession time, considering gravity, as a function of the vertical magnetic field gradient. S_z is the mean vertical spin component averaged over all UCN exiting the precession chamber.

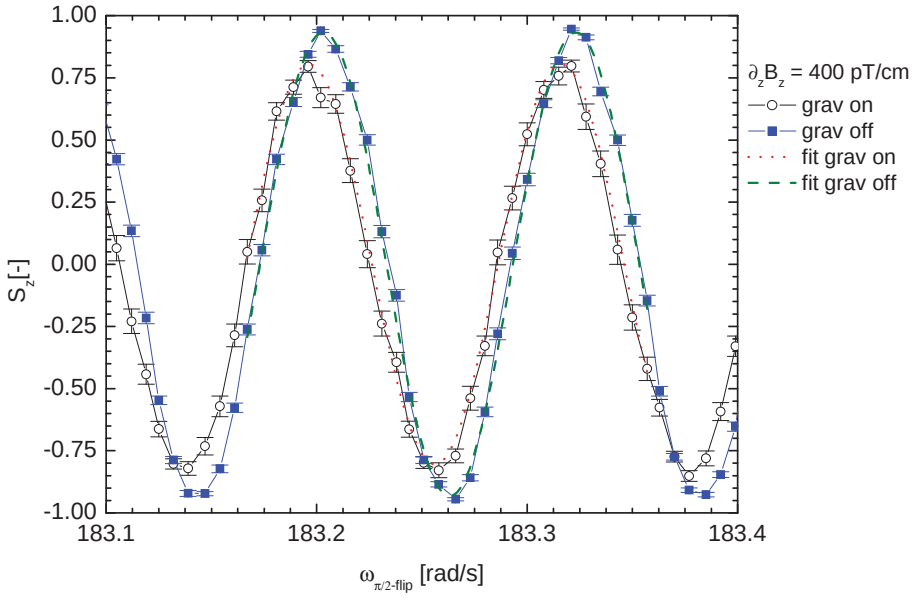

Fig.9: Zoom around the Ramsey resonance frequency for 50 s precession time and 400 pT/cm vertical magnetic field gradient with gravity on and off. The frequency shift due to gravity is in agreement with analytical prediction (see text).

5. Conclusions and plans

The MCUCN code proved to be a reliable tool by giving a good agreement with measured filling, storing and emptying curves of the nEDM apparatus. The described MC fitting procedure is being further developed to work faster also for applications with new data to be obtained with the nEDM apparatus at the PSI source.

By using the newly developed spin handling features in MCUCN, future simulations will serve as consistency tests and as means to estimate several systematic effects due to gravity, magnetic field gradients (dipoles, quadrupoles), and **v×E** effects [8].

MCUCN is available for the UCN physics community, see MC website [11].

References

[1] C.A. Baker *et al.*: these proceedings.
[2] C.A. Baker *et al.*: Phys. Rev. Lett **97**, 131801 (2006).
[3] R. Golub *et al.*: Ultra-Cold Neutrons, IOP Publishing (1991).
[4] A. Steyerl: Zeitschrift für Physik **A 254**, 169 (1972).
[5] A. Steyerl: PhD thesis, Technische Universität München (1971).
[6] M. Kuzniak: PhD thesis, Jagiellonian University (2008).
[7] A. Knecht: PhD thesis, Universität Zürich (2009).
[8] J. Pendlebury *et al.*: Phys. Rev. **A 70**, 032102 (2004).
[9] K. Bodek *et al.*: NIM **A597**, 222 (2008).
[10] http://www.cyfronet.pl/en/
[11] http://ucn.web.psi.ch/mc/